One-dimensional Bose gas on an atom chip

van Amerongen, A.H.

4 Realizing Bose-Einstein condensation

4.1 Introduction

This chapter describes one trapping and cooling cycle that is used to reach Bose-Einstein condensation (BEC) in the microtrap that was described in Ch. 3. The first part (Sec. 4.2) describes the magneto-optical cooling steps and a rapid evaporative cooling stage that we apply to reach an elongated three-dimensional BEC. Section 4.2.7 describes the specific scheme that was used to reach the cross-over to the 1D quasi-condensate regime. In Sec. 4.3, we characterize the roughness of the trapping potential for our quasi-condensates. This roughness stems from non-straight current flow in the trapping wire. We discuss how we have reduced the influence of this roughness and we give an estimate for the smoothness of the resulting potential.

4.2 Trapping and cooling sequence

Our goal in the trapping and cooling sequence is to reach quantum degeneracy with the highest atom number possible. A spherical gaussian cloud of radius r containing N atoms has a central density $n_0 = N\pi^{-3/2}r^{-3}$. The phase space density in the trap center is $\Phi = n_0\Lambda_T^3$, with Λ_T the thermal de Broglie wavelength, Eq. (2.14). Bose-Einstein condensation in a three-dimensional ideal Bose gas is reached for $\Phi > 2.612$ (see Ch.2). The successive steps, discussed here, that increase the phase space density of a cloud of atoms and finally lead to Bose condensation are generally applied in BEC labs worldwide. Specific for our experimental setup is the use of miniwires to generate the magnetic potentials for the cooling and trapping stages. In short, the procedure is as follows. In the first step we load our mirror-MOT [111] secondly we apply a short compressed MOT [125] stage. Subsequently the atoms are optically pumped to a single magnetic Zeeman state followed by magnetic trapping in the miniwire trap. A transfer to the magnetic potential of the on-chip Z-wire enables us to compress the trapping volume thereby increasing the inter-atomic collision rate. Finally, we perform forced evaporative cooling using radio frequency induced spin flips. A single 1.2 s RF ramp leads to the fast and relatively efficient production of a Bose-Einstein condensate of $\sim 10^4$ atoms. These steps are described below in more detail.

4.2.1 MOT

We start the trapping and cooling sequence by resistively heating the dispenser described in Sec. 3.6. The hot ($T > 600$ °C) rubidium atoms that escape from the dispenser thermalize by collisions with the walls of the vacuum chamber. At room temperature and a ^{87}Rb pressure of 10^{-9} mbar we have $\Phi = 10^{-25}$. The largest gain in phase space density is reached in the first cooling step with the magneto-optical trap (MOT): We trap $5 \cdot 10^7$ atoms and reach $\Phi = 10^{-9}$. Specifically, we use the mirror MOT [111] configuration (see Sec. 3.3), where four cooling laser beams with 15 mm $1/e^2$ diameter and 9 mW of power per beam impinge on the central trapping area (see Fig. 3.2). The two beams in the yz-plane reflect at a 45° angle on the surface of our micro-electronic chip. This scheme creates the three orthogonal beam pairs needed for a 3D MOT while the center of the MOT is only millimeters away from the chip surface. The cooling light is detuned 2.7 Γ to the red with respect to the $F = 2 \rightarrow F = 3$ cycling transition of the D2-line and the central intensity is $6I_0$, where the saturation intensity is $I_0 = 1.67$ mW/cm^2 and $\Gamma/2\pi = 6$ MHz is the natural linewidth of the atomic transition. We overlap a repumper light beam with the same diameter with all four cooling beams. The repumper is resonant with the $F = 1 \rightarrow F = 2$ transition of the D1-line, and the central intensity is at saturation (1.49 mW/cm^2). The quadrupole magnetic field in this initial stage is generated with the MOT coils (Sec. 3.7) that produce a gradient of 15 G/cm. The dispenser, see Sec. 3.6, is pulsed on by resistive heating during a 4 s 12 A current pulse. After switching off the current, the dispenser cools down within 4 s. The vacuum pressure recovers for 6 s after the end of the dispenser pulse before we prepare for the second cooling step by transferring the atoms to a miniwire-based MOT. A schematic overview of the cooling and trapping sequence described here is shown in Table 4.1. We ramp down the current in the MOT coils while ramping on current in the miniwires in combination with a homogeneous bias field of 5 G in the $+y$ direction. A -4 G bias field component in the z direction is added to match the ideal quadrupole field optimally [126]. The miniwires and their dimensions are shown in Fig. 3.3. In the positive x direction miniwires 4, 5, and 6 carry a current of 2 A each, while miniwires 1 and 3 are operated at +3.5 A and -3.5 A along y respectively. The transfer takes 80 ms and the resulting miniwire quadrupole field compresses the MOT magnetic field to a gradient of 30 G/cm at a distance of 1.2 mm from the chip.

4.2.2 Compressed MOT

The next important increase in phase space density is achieved with the compressed MOT technique [125]. In this 6 ms cooling stage we reduce the light pressure, that arises from the scattered cooling photons, by decreasing the repumper intensity by two orders of magnitude while we increase at the same time the detuning of the cool light from 2.7 Γ to 13 Γ. Consequently a larger fraction of the the MOT atoms will end up in the dark $F = 1$ ground state, hence the alternative nomenclature for this trick: "transient dark MOT". The compressed MOT stage results in a

	MOT loading	Vacuum recover	compress+move up	wire MOT	compressed MOT		optical pumping	mini wire IP trap	Z-wire trap	compress Z	evaporative cooling
Dispenser											
MOT coil 1											
MOT coil 2											
bias coil By											
mini-wires 4,5,6											
mini-wires 1,3											
miniwire 2											
chip Z-wire											
RF											
cool light											
Repumper											
Pump											
detuning/(2π6MHz)	2.7	2.7	5.5	2.7	13	0					
duration [ms]	4000	6000	80	105	6	0.4	10	38	400	1200	
atom number [10^6]	50	50	50	40	40	40	20	20	20	0.04	
temperature [μK]	100	100	100	100	100	30	40	40	500	1.3	

Table 4.1: Timeline for the trapping and cooling sequence. In the first step we load our mirror-MOT, secondly we apply a short compressed MOT stage. Subsequently the atoms are optically pumped to a single magnetic Zeeman state followed by magnetic trapping in the miniwire trap. A transfer to the magnetic potential of the on-chip Z-wire enables us to compress the trapping volume thereby increasing the inter-atomic collision rate. Finally, we perform forced evaporative cooling using radio frequency induced spin flips. A single 1.2 s RF ramp leads to the fast and relatively efficient production of a Bose-Einstein condensate.

dense cold cloud with a lower atom number but a much higher phase space density ($N = 4 \cdot 10^7$; $T = 30$ μK; $n_0 = 5 \cdot 10^{16}$ m^{-3}; $\Phi = 2 \cdot 10^{-6}$) compared to the standard MOT.

4.2.3 Optical pumping

An optical pumping stage transfers the atoms to the magnetically trappable $F = 2, m_F = 2$ Zeeman state. First the MOT light and quadrupole field are switched off. A small bias field, $B_y = 2$ G defines a quantization axis for the atoms. Two co-linear circularly polarized beams also point in the y direction: a resonant repump beam (D1; $F = 1 \rightarrow F = 2$) and the pump beam, tuned to the $F = 2 \rightarrow F = 2$ transition of the D2-line. An optical pumping pulse of 400 μs at an intensity ~ 3 mW/cm^2 per beam transfers nearly all atoms to the doubly polarized state.

4.2.4 Minitrap

The spin-polarized atoms can now be captured in the Ioffe-Pritchard magnetic trap. To exactly mode match the optically cooled cloud ($T = 30$ μK) with a radius ($r \approx 0.5$ mm) to the trapping potential we need trap frequencies $\omega = \sqrt{2k_BT/mr^2} =$

$2\pi \times 23$ Hz. These low frequencies can only be reached in a chip trap that is very shallow due to gravitational sag. Our best results ($N = 2 \cdot 10^7; \Phi = 1 \cdot 10^{-6}$) were achieved by lifting the trap bottom B_0 to 8 G resulting in a trap with an axial frequency of 16 Hz and a radial frequency of 46 Hz. Miniwire current settings are: 6.65 A, for wires 4,5 and 6; 9.8 A, for wires 1 and 3, and -2.5 A through miniwire 2. The cartesian field vector from the external bias coils is $(B_x, B_y, B_z) = (8, 17, 0)$ G.

4.2.5 Z-trap – compression

After having loaded the miniwire trap we start a magnetic field ramp that adiabatically transfers the atoms to a potential made with the on chip Z-wire. The Z-wire current is ramped to 2.25 A in 28 ms while the miniwires are turned off. In order to increase the axial harmonic confinement frequency we leave on miniwire 2 (see Fig. 3.3) with -2 A of current. We adiabatically compress the cloud in two steps. We ramp down B_0 (in the x direction) from 8 G to 2.2 G in 400 ms while in the last 200 ms we also increase B_y from 17 G to 40 G. After this transformation the trap frequencies are $\omega_{\|} = 2\pi \times 35$ Hz in the axial and $\omega_{\perp} = 2\pi \times 3.3$ kHz in the radial direction.

4.2.6 Reaching BEC by evaporative cooling

The final increase in phase space density of six orders of magnitude that ultimately leads to degeneracy is achieved by evaporative cooling [98,99]. In Sec. 2.8 a treatment of the evaporative cooling process along the lines of [99] is given for the specific case of our IP trap, in the regime where the confining potential is radially linear and axially harmonic. We selectively remove the high-energy tail of the Maxwell-Boltzmann velocity distribution of the trapped atoms using radio-frequency (RF) induced spin flips. Hot atoms are resonantly excited with a RF signal from a DDS (Sec. 3.10.2) that is connected to a chip wire neighboring the Z-trap wire. For our starting condition ($N = 2 \cdot 10^7$; $\Phi = 1 \cdot 10^{-6}; T \approx 45$ μK) the elastic collision rate, Eq. (2.56), $1/\tau_{\rm el} = 4$ s^{-1}. By adiabatic compression of the IP-trap at constant atom number we reduce the trap volume with a factor $\beta \approx 140$, thereby boosting the scatter rate by that same factor ($1/\tau_{\rm el} \propto \beta$). In this case the temperature scales as $T \propto \sqrt{\beta}$, and goes up to ≈ 0.6 mK. As our trap, with depth $\epsilon = 38$ G (2.5 mK), is not quite deep enough to maintain $\eta > 7$ needed for a $\gamma_{\rm e} > 2$ (see Fig. 2.5), we apply an evaporation knife at a constant height of 38.5 G ($\omega_{\rm RF}/2\pi$ =27 MHz, $\epsilon = 36.3$ G) during the adiabatic compression ramp, to guarantee homogeneous evaporation at all times.

After compression we start a logarithmic frequency sweep from 27 MHz to a final value of ~ 1.55 MHz with a duration of 1.2 s. Condensation is reached at an atom number of $7 \cdot 10^4$ and a temperature of 1.3(1) μK. The central density at condensation is $3 \cdot 10^{20}$ m^{-3} leading to a scatter rate of $3 \cdot 10^3$ s^{-1}. The overall efficiency is $\gamma_{\rm e,tot} = 2.6$. In Fig. 4.1 (left) we show absorption images taken on the day that the first condensates were produced in our setup in the spring of 2006. Pictures are taken after 11 ms of free expansion and correspond to lowering the RF

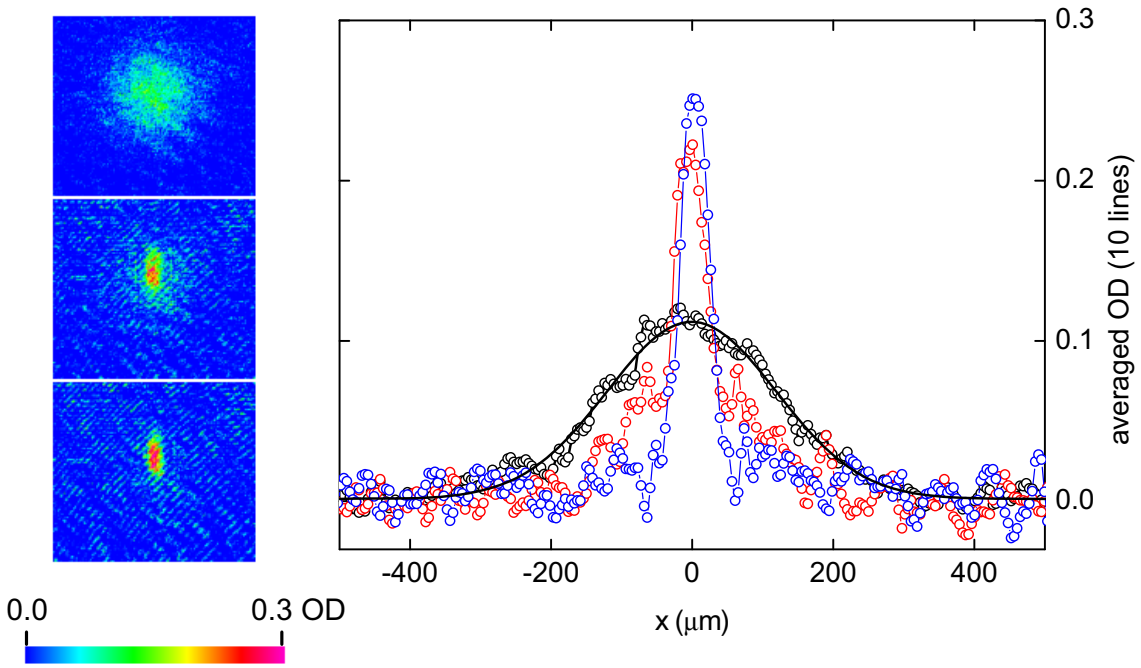

Figure 4.1: (left) Absorption images of ultracold atom clouds, taken after 11 ms of free expansion, correspond to lowering the RF evaporation knife from 1.63 MHz (top) to 1.59 MHz (middle) and finally 1.57 MHz (bottom). (right) horizontal cut through the displayed absorption images. A clear transformation from the gaussian thermal distribution above T_c (○) to a bimodal distribution (○), and finally the Thomas-Fermi shape of an almost pure condensate (○). The black line corresponds to a gaussian fit to the data at 1.63 MHz, the temperature resulting from this fit is 1.4(1) μK.

evaporation knife from 1.63 MHz (top) to 1.59 MHz (middle) and finally 1.57 MHz (bottom). The panel at the right in Fig. 4.1 shows a horizontal cut through the displayed absorption images. A clear transformation is visible from the gaussian thermal distribution above T_c (○) to a bimodal distribution (○), and finally the Thomas-Fermi shape of an almost pure condensate (○).

4.2.7 Axial relaxation – reaching BEC in the 3D-1D cross-over

For the experiments on the Bose gas in the dimensional cross-over regime from 3D to 1D that are described in Ch. 5 and Ch. 6 we have used the following adapted procedure. After the first 400 ms of compression of the Z-wire trap we start a linear evaporation ramp of 600 ms from 27 MHz to 1.7 MHz. Before reaching degeneracy we relax the axial confinement to a final trap with $\omega_\parallel/2\pi = 8.5$ Hz along x, and $\omega_\perp/2\pi = 3280$ Hz, and a bottom corresponding to $\omega_{RF}/2\pi = 1.518(2)$ MHz; for comparison $\hbar\omega_\perp/k_B = 158$ nK. The current in the Z-wire is set at 2.25 A, and the distance of the cloud to the chip surface is 90 μm. In this final trap a slower forced

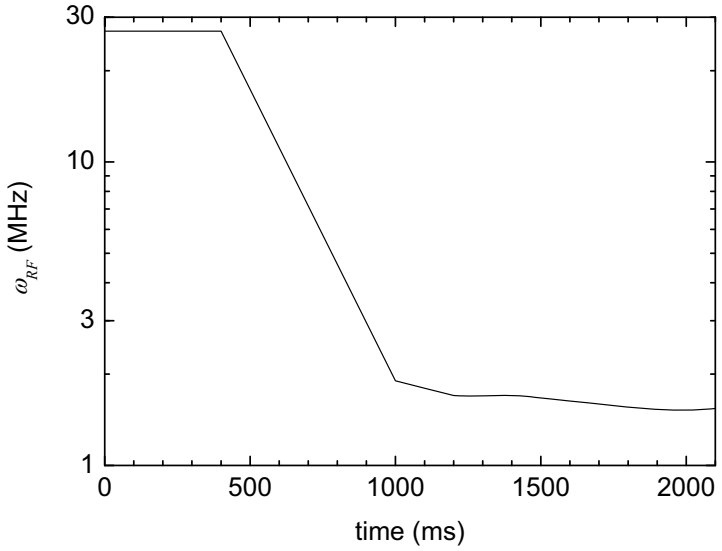

Figure 4.2: RF frequency ramp that was employed for the achievement of an elongated condensate. We start by applying 400 ms of plain evaporation during the compression of the magnetic trap. Followed by a rapid cooling ramp (600 ms) before we carefully relax the trap axially and cool to degeneracy slowly in order to create an elongated condensate that is in equilibrium at the end of the last 300 ms of plain evaporation.

evaporation stage is performed, where we ramp the RF frequency from 1.7 MHz to $\sim$ 1.55 MHz in 450 ms. An additional 300 ms of plain evaporation at the final RF frequency allows the damping of residual quadrupole collective oscillations in the cloud to the point where these oscillations are no longer visible within our experimental resolution. We slow down the evaporation process before reaching BEC to avoid shock cooling: if the cooling goes faster than the axial thermalization, local patches of BEC are formed along the axis. These patches subsequently collapse into the central potential resulting in large quadrupole oscillations [127]. We reach degeneracy at an atom number of $4 \cdot 10^4$, thus the overall efficiency is $\gamma_{\mathrm{e,tot}} = 2.2$. The RF ramp is shown in Fig.4.2. To penetrate further into the 1D regime we can purposely reduce the atom number by performing the first RF ramp from 27 MHz to 1.7 MHz much faster, for example not in 600 ms but in 160 ms. In the latter case the linear density of a quasi-condensate is 50 $\mu\mathrm{m}^{-1}$, well below the cross-over value of 150 $\mu\mathrm{m}^{-1}$ (see 2.4.3).

4.3 Potential roughness

Our typical trapping distance $d = 90$ μm is of the same order as the typical axial size of a cold cloud. At this relatively large distance the effect of potential corrugations due to wire roughness at large spatial frequencies ($\gg 1/d$) is strongly suppressed [128, 129]. Only residual, long-wavelength ($\lambda \sim d$) deviations from straight

current flow in the trapping wire are visible as small (< 1 mG) potential perturbations. The relative potential roughness is $\Delta B/B \sim 10^{-5}$. This roughness corresponds to a few tens of nanokelvins in energy and thus disturbs our condensates that have a chemical potential of ~ 160 nK. In order to minimize the effect of the residual wire corrugations we look for a "sweet spot" along the trap axis. We displace the trap center in the x direction by sending additional currents through miniwires 1 ($-y$) and 3 ($+y$). The resulting magnetic field gradient gives an approximately linear displacement of 400 μm/A. In Fig. 4.3 a scan along the x-axis is shown, subsequent traces are shown displaced in the vertical direction to increase the visibility. Linear density traces are taken for increasing miniwire current in steps of 50 mA, corresponding to approximately 20 μm axial displacement per step. The red curve is taken in a region where the potential is smoothest: our sweet spot.

After the identification of the sweet spot we have characterized the axial trapping potential with standard methods using both the measurement of *in situ* density profiles at high T [129] and the dipole mode oscillation frequency in the trap center. The relative potential roughness at $d = 90$ μm is $\Delta B/B \sim 10^{-5}$ and can be compared to the value of $\Delta B/B \sim 10^{-5}$ quoted by Krüger *et al.*, be it much closer to the chip ($d = 10$ μm) [130]. Our potential is much smoother than the original trap wire used by the Orsay group that was nicely characterized in Ref. [129].

Note that we have followed here a pragmatic approach to circumvent the effect of wire corrugations. For the present work, a full analysis of the cause of the irregular cloud shapes in Fig. 4.3 was not performed. Another way to suppress potential roughness was presented in Ref. [131]. There, a new method for strong suppression of the corrugation (employing ac modulation) was demonstrated. Evidence for strong suppression of the corrugation was obtained from the increase of the damping time of the center-of-mass motion, while the optical images still showed some residual apparent roughness in the 10-nK range. This apparent roughness was attributed to residual noise in the imaging system.

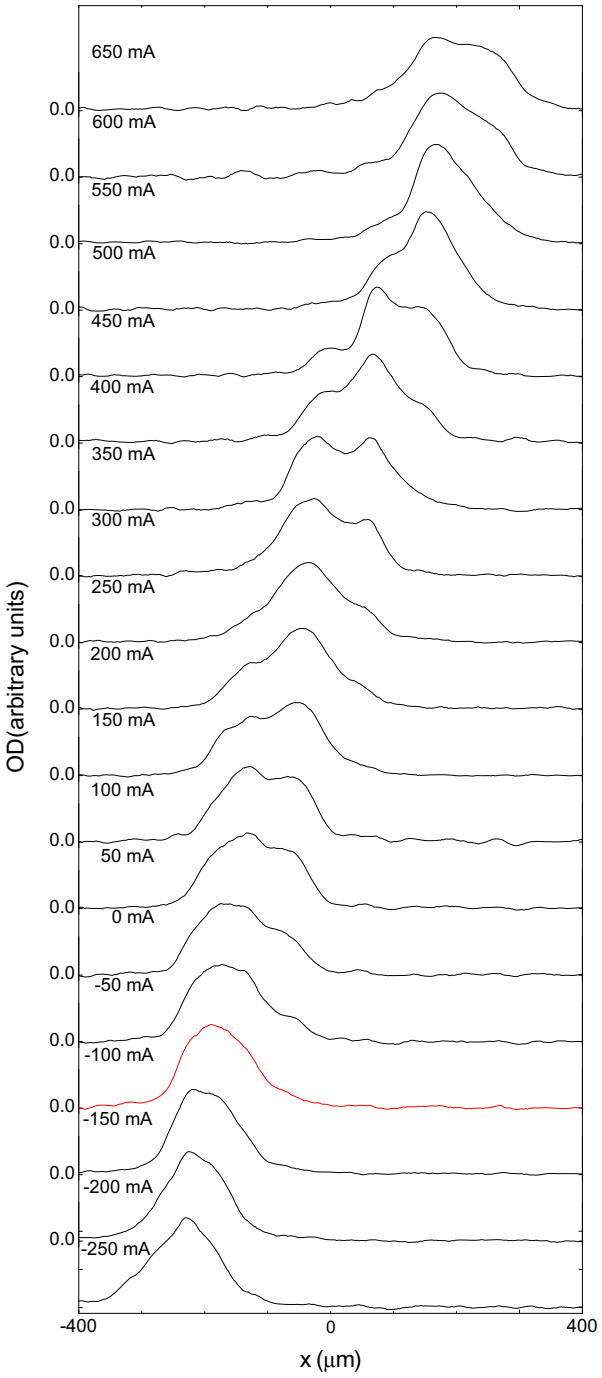

Figure 4.3: Linear density traces of condensates imaged *in situ* for varying axial trap center position. Traces are taken for increasing miniwire 1 and 3 current with steps of 50 mA, corresponding to approximately 20 μm axial displacement. In the graph subsequent traces are displaced vertically to increase the visibility. The red curve indicates our "sweet spot", the region where the potential is smoothest.